

NONLINEAR OPTICAL PHENOMENA

https://doi.org/10.1070/QEL17494

Nonlinear optical absorption in thin halide perovskite films under femtosecond excitation at wavelengths of 1064 and 532 nm

D.V. Khudyakov, D.V. Ganin, A.D. Lyashedko, L.A. Frolova, P.A. Troshin, A.S. Lobach

Abstract. **The nonlinear optical responses of perovskite films $CsPbI_2Br$, $MAPbI_3$ + 1% PVC, $MA_{0.15}FA_{0.75}Cs_{0.1}PbI_{2.85}Br_{0.15}$, and $MA_{0.15}FA_{0.75}Cs_{0.1}PbI_3$, irradiated by femtosecond laser pulses with wavelengths of 1064 and 532 nm, are investigated using *z*-scan measurements. Nonlinear absorption is found to occur in perovskite films irradiated at a wavelength of 1064 nm; the nonlinear absorption coefficient in thin films (45–65 nm) greatly exceeds that in thick ones (120–350 nm): 524–928 and 38–50 cm GW^{-1}, respectively. It is shown that the nonlinear absorption saturation intensity for perovskite films depends on the pump pulse duration and increases with pulse shortening. It is also established that the nonlinear absorption coefficient of organometallic perovskite films exceeds that of a film of inorganic perovskite $CsPbI_2Br$. Bleaching of film samples during *z*-scanning at a wavelength of 532 nm is related to the irreversible photochemical degradation of films exposed to intense light. The kinetics of photochemical bleaching of the films is detected at a wavelength of 532 nm.**

Keywords: *organometallic halide perovskites, thin perovskite films, semiconductor materials, nonlinear optical absorption, two-photon absorption.*

1. Introduction

Organometallic halide perovskites attract close attention of researchers because of their remarkable optical and electronic properties, which are used primarily in solar cells and converters of electrical energy into light. New hybrid perovskites, since the time they were discovered (in 1880), have been described by the general chemical formula ABX_3, proposed for the first time in 1978 for the compound $MAPbX_3$, where MA is the methylammonium cation and X is the halide anion [1–3]. Metal–halide perovskites, as follows from their name, consist of an inorganic halide (I^-, Cl^-, Br^-), which occupies the site of monovalent anion X, and a divalent metal cation (Pb^{2+}, Sn^{2+}, or Ge^{2+}), denoted by the letter B. An organic or inorganic monovalent cation A^+ can form, respectively, inorganic (A is an inorganic cation) or hybrid (A is an organic cation) metal–halide perovskites. A conventionally used inorganic cation is Cs^+; popular organic ones are cations of methylammonium ($MA^+ = CH_3NH_3^+$), formamidinium [$FA^+ = CH(NH_2)_2^+$], etc.

Perovskite materials are known to possess high photovoltaic efficiency, adjustable band gap, high lifetime of photoexcited carriers, and high fluorescence quantum yield. At the same time, they are characterised by a significant nonlinear optical response. As was found in [4], the nonlinear absorption coefficient of perovskite materials in the near-IR range is several orders of magnitude higher than that of conventional semiconductors, for example, Si, ZnSe, and CdSe. Thin films of perovskites $MAPbI_3$ were used as a saturable absorber for mode locking in a pulsed fibre laser at a wavelength of 1064 nm [5] and for *Q*-switching in a neodymium laser at a wavelength of 1060 nm [6]. In [7, 8], the nonlinear properties of thin perovskite films were found to depend on the type of the crystal structure formed during their synthesis, and a significant increase in the nonlinear response when passing from bulk samples to the nanocrystalline structure of these films was demonstrated. It was revealed that a saturable absorber based on two-dimensional perovskite nanosheets exhibits a higher nonlinear response with a large modulation depth and very low saturation intensity as compared with bulky perovskite samples. At the same time, perovskite materials are easily destroyed under the action of air oxygen and moisture, high temperature, and illumination, which is a hindrance for their technological application. Thus, additional studies should be performed to develop methods for increasing the resistance and long-term stability of perovskites under environmental impacts. Depending on the experimental conditions (probe wavelength, pulse duration) and type of the perovskite material (chemical structure, crystalline morphology), the values of nonlinear absorption coefficient and saturation intensity may differ by several orders of magnitude. In this paper, we report the results of studying the nonlinear response of perovskite films in dependence of their chemical structure, the radiation intensity, and the excitation pulse duration.

2. Experimental

The objects of study were perovskites with the best-to-date thermal stability and photostability: hybrid halide perovskites doped with polyvinylcarbazole (PVC), $MAPbI_3$

D.V. Khudyakov, D.V. Ganin Physics Instrumentation Centre, Prokhorov General Physics Institute of the Russian Academy of Sciences, Kaluzhskoe sh., 40-i km, 108840 Troitsk, Moscow, Russia; e-mail: dimakh65@gmail.com;
A.D. Lyashedko Optosystems Ltd., Kaluzhskoe sh., 40-i km, 108840 Troitsk, Moscow, Russia;
L.A. Frolova, P.A. Troshin Skolkovo Institute of Science and Technology, ul. Nobelya 3, 143026 Moscow, Russia; Institute of Problems of Chemical Physics, Russian Academy of Sciences, prosp. Akad. Semenova 1, 142432 Chernogolovka, Moscow region, Russia;
A.S. Lobach Institute of Problems of Chemical Physics, Russian Academy of Sciences, prosp. Akad. Semenova 1, 142432 Chernogolovka, Moscow region, Russia

Received 27 November 2020
Kvantovaya Elektronika **51** (3) 211–216 (2021)
Translated by Yu.P. Sin'kov

+ 1% PVC [9], perovskites with ternary mixed organometallic cation ($MA_{0.15}FA_{0.75}Cs_{0.1}PbI_3$) [10], perovskites with mixed ternary organometallic cation and halide anions ($MA_{0.15}FA_{0.75}Cs_{0.1}PbI_{2.85}Br_{0.15}$) [11], and completely inorganic perovskite with mixed halide anions ($CsPbI_2Br$) [12].

2.1. Preparation of samples and their characteristics

Synthesis of perovskite materials and subsequent deposition of perovskite films and polymers on glass substrates were performed in a box with inert atmosphere ($[H_2O] < 0.1$ ppm, $[O_2] < 0.1$ ppm). The glass substrates ($25 \times 25 \times 1$ mm) were previously washed in solvents (toluene and acetone) and then processed in UV plasma for 5 min.

Perovskite films of methylammonium iodoplumbate $MAPbI_3$ + 1% PVC, modified with a polyvinylcarbazole-based polymer additive, were obtained by spin-coating, a method described by us previously in [9].

Perovskite films $MAPbI_3$ + 1% PVC were spin-coated on purified glass substrates from a solution of 0.45 M $CH_3NH_3PbI_3$ in anhydrous dimethylformamide (DMF), with 1 wt % PVC added (substrate rotational speed 3000 rpm, deposition time 50 s). To obtain optimal morphology, 120 μL of toluene were added at the film centre 8 s after depositing the perovskite precursor. Then the films were annealed at 100 °C for 10 min. The $MAPbI_3$ + 1% PVC films were ~65-nm thick.

Perovskite films of caesium formamidinium methylammonium iodobromoplumbate $MA_{0.15}FA_{0.75}Cs_{0.1}PbI_{2.85}Br_{0.15}$ were spin-coated (6000 rpm, 50 s) from a solution of 1.4 M $MA_{0.15}FA_{0.75}Cs_{0.1}PbI_{2.85}Br_{0.15}$ in a mixture of anhydrous DMF and dimethyl sulfoxide (DMSO), with a volume ratio of 4 : 1. To obtain optimal morphology, 40 μL of toluene were added at the film centre 22 s after the perovskite precursor deposition. Then the films were annealed at 100 °C for 5 min. The thickness of $MA_{0.15}FA_{0.75}Cs_{0.1}PbI_{2.85}Br_{0.15}$ films was ~350 nm.

Perovskite films of caesium formamidinium methylammonium iodoplumbate $MA_{0.15}FA_{0.75}Cs_{0.1}PbI_3$ were spin-coated (6000 rpm, 60 s) from a solution of 0.3 M $MA_{0.15}FA_{0.75}Cs_{0.1}PbI_3$ in a mixture of anhydrous DMF and DMSO with a volume ratio of 4 : 1. To implement optimal morphology, 40 μL of toluene were added at the film centre 30 s after the perovskite precursor deposition. The $MA_{0.15}FA_{0.75}Cs_{0.1}PbI_3$ films were ~45- and 55-nm thick.

Perovskite films of caesium iodobromoplumbate $CsPbI_2Br$ were spin-coated (1200 rpm, 50 s) from a solution of 0.4 M $CsPbI_2Br$ in anhydrous DMF and annealed at 265 °C for 2 min. The $CsPbI_2Br$ film was ~120-nm thick.

To prevent perovskite films from possible decomposition under the action of air moisture and oxygen in subsequent measurements, they were covered with a thin polymethylmethacrylate (PMMA) layer. PMMA films were spin-coated (3000 rpm, 50 s) from a solution with a concentration of 50 mg mL^{-1} in toluene. Opaque hermetic packing (foil) was used to store and transport perovskite materials; storage was performed in an inert atmosphere. Before carrying out experiments with laser irradiation, films were extracted from packing, and measurements were carried out in air for no more than 2–3 min. The reproducibility of measurement results, as well as the optical properties (spectra) of films during experiment served a measure of their stability. The absorption spectra of perovskite films on glass were recorded using a Shimadzu UV-3101 PC UV-Vis-NIR scanning spectrophotometer (Japan). The glass background absorption was subtracted. The structural characteristics of perovskites were studied by X-ray diffraction on a Bruker D8 diffractometer (Germany) (CuK_α radiation). The surface morphology of perovskite films was investigated on a Zeiss LEO SUPRA 25 scanning electron microscope (Germany). The characteristics obtained coincided with the data in the literature. The thicknesses of perovskite films were measured with an atomic-force microscope.

2.2. *Z*-scan measurements at a wavelength of 1064 nm

The nonlinear optical characteristics of perovskite films on glass were measured using the *z*-scan method. A 1064-nm pulsed Yb^{3+} fibre laser with a pulse repetition rate of 10 kHz served as a probe one. The pulse duration and energy were, respectively, 400 fs and 1.5 μJ. Longitudinal (*z*) scanning was performed according to the standard scheme without a diaphragm: only nonlinear absorption was recorded. The laser beam was focused by a lens with a focal length of 12 cm. The waist radius at an intensity level of e^{-2} was 28 μm. The samples under study (perovskite films on a glass plate) were installed on a translation stage, which could be moved along the laser beam axis (*z* coordinate) near the focal region. The peak intensity of incident beam in the waist was calculated from the formula

$$I_0 \approx \frac{E_p}{\pi r_0^2 \tau_0}, \quad (1)$$

where E_p is the laser pulse energy incident on a sample, r_0 is the waist radius at the level of e^{-2}, and τ is the laser pulse duration (FWHM of the intensity profile). Neutral filters were installed at the laser output in order to vary the pulse energy E_p in the range from 10 to 1500 nJ. The measurable parameter was transmittance *T*: the ratio of the average power transmitted through the sample to the incident power. Figure 1 shows the experimental *z*-scan signals obtained when probing the sample $MAPbI_3$ + 1% PVC at a wavelength of 1064 nm.

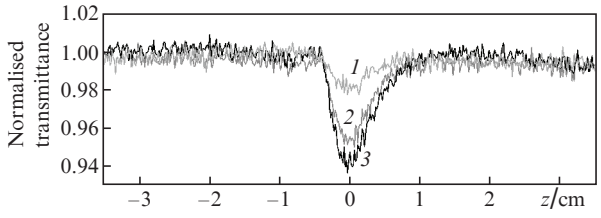

Figure 1. Experimental *z*-scan signals for the 65-nm-thick $MAPbI_3$ + 1% PVC film at a probe wavelength of 1064 nm and pulse energies of (*1*) 122, (*2*) 202, and (*3*) 330 nJ.

The absorption in the region of the laser beam waist increases with increasing intensity, due to which the transmittance near the coordinate $z = 0$ decreases. A similar decrease in transmittance with an increase in the beam intensity was observed for the $CsPbI_2Br$, $MA_{0.15}FA_{0.75}Cs_{0.1}PbI_3$, and $MA_{0.15}FA_{0.75}Cs_{0.1}PbI_{2.85}Br_{0.15}$ samples probed at a wavelength of 1064 nm. Their transmittance spectra (see Fig. 2) do not exhibit any significant absorption at the lasing wavelength (1064 nm), whereas the absorption significantly increases at the second harmonic wavelength (532 nm). The

band gap of the semiconductors under study is E_g = 1.49–1.79 eV, a value exceeding the photon energy E = 1.16 eV at the wavelength of 1064 nm. At the same time, in the case of two-photon absorption (TPA), charge photoseparation and electron transfer to the conduction band become possible (see Fig. 3). Specifically TPA made the main contribution to the nonlinear absorption at a wavelength of 1064 nm in our experiments. The experimental data were interpreted using the analytical expressions derived for the main experimental dependences. The transitions of photoexcited carriers between the valence and conduction bands in the two-photon process were described within the two-level model (Fig. 4).

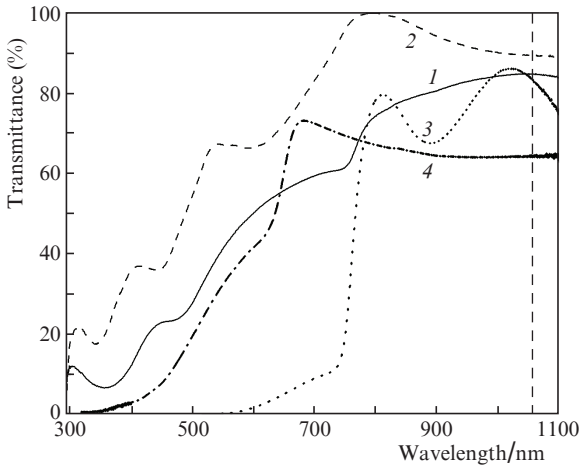

Figure 2. Optical transmittance spectra of (*1*) $MAPbI_3$ + 1% PVC, (*2*) $MA_{0.15}FA_{0.75}Cs_{0.1}PbI_3$, (*3*) $MA_{0.15}FA_{0.75}Cs_{0.1}PbI_{2.85}Br_{0.15}$, and (*4*) $CsPbI_2Br$ perovskite films. The vertical dashed line corresponds to the lasing wavelength 1064 nm.

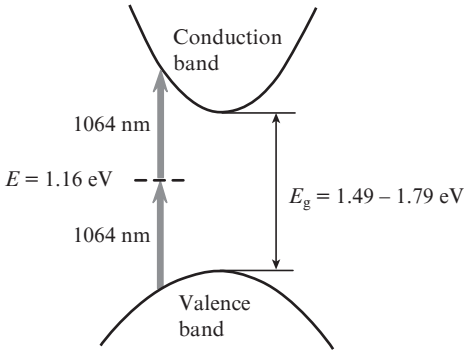

Figure 3. Schematic diagram of energy bands and transitions for two-photon absorption in perovskite samples.

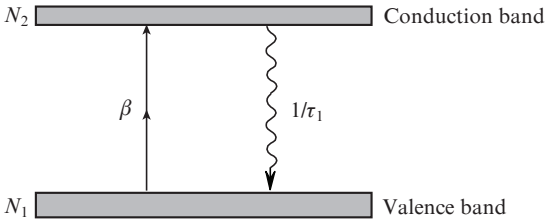

Figure 4. Two-level model for describing the kinetics of two-photon transitions in perovskite samples.

The equation for the rate of change in the electron concentration in the valence band has the form

$$\frac{dN_1}{dt} = \frac{N_2}{\tau_1} - \frac{\beta}{2h\nu} I_0^2, \tag{2}$$

where β is the TPA coefficient; N_1 and N_2 are the electron concentrations in the valence and conduction bands, respectively; τ_1 is the recombination time of photoexcited carriers; I_0 is the probe peak intensity; and ν is the probe frequency. When integrating Eqn (2), the integration limits are determined by the probe pulse duration τ_0, which is much shorter than the recombination time of photoexcited carriers: τ_1 = 250–1000 ns [13]; therefore, the term N_2/τ_1 in the right-hand side of (2) can be neglected. In this case, on the assumption that the light pulse has a Gaussian profile, integration of Eqn (2) yields the following relation for the concentration N_1 immediately after the end of excitation pulse:

$$N_1 = N_0 - \frac{\beta}{h\nu} I_0^2 \tau_0 K, \tag{3}$$

where N_0 is the initial electron concentration in the valence band before the probe pulse arrival and $K = \sqrt{\pi}(4\sqrt{2\ln 2})^{-1} \approx 0.376$. Using the expression

$$\sigma = \frac{\beta h\nu}{N_1} \tag{4}$$

for the TPA cross section and substituting N_1 from (4) into (3), we obtain the relation for the dependence of TPA coefficient on the incident intensity:

$$\beta = \frac{\beta_0}{1 + (I_0/I_s)^2}, \tag{5}$$

where

$$I_s^2 = \frac{(h\nu)^2}{\sigma\tau_0 K} \tag{6}$$

is the squared TPA saturation intensity and $\beta_0 = \sigma N_0/(h\nu)$ is the TPA coefficient at beam intensities much lower than the saturation intensity. The dependence of the nonlinear absorption of a sample involved in a two-photon process on the longitudinal coordinate z is described by the equation

$$\frac{dI}{dz} = -\beta I^2, \tag{7}$$

where I is the radiation intensity. Solving Eqn (7), we arrive at the expression for the transmittance T in dependence of the incident intensity and sample thickness L:

$$T(I_0) = \frac{I_1}{I_0} = \frac{1}{1 + \beta L I_0}, \tag{8}$$

where I_1 is the intensity transmitted through the sample. Let us rewrite (8) [having replaced β with expression (5) in order to take into account the TPA saturation] in the form

$$T(I_0) = \left[1 + \frac{\beta_0 L I_0}{1 + (I_0/I_s)^2}\right]^{-1}. \tag{9}$$

Figure 5 shows the experimental dependences of normalised transmittance on the peak intensity I_0 for the perovskites $MA_{0.15}FA_{0.75}Cs_{0.1}PbI_3$, $MAPbI_3$ + 1% PVC, and $CsPbI_2Br$, which were determined from the experimental z-scan curves at $z = 0$. The experimental dependences were approximated using expression (9); the best approximation yielded the values of nonlinear coefficient β_0 and saturation intensity I_s. The experimental results obtained with the aid of Eqn (9) are listed in Table 1, which also contains data from other sources known to date.

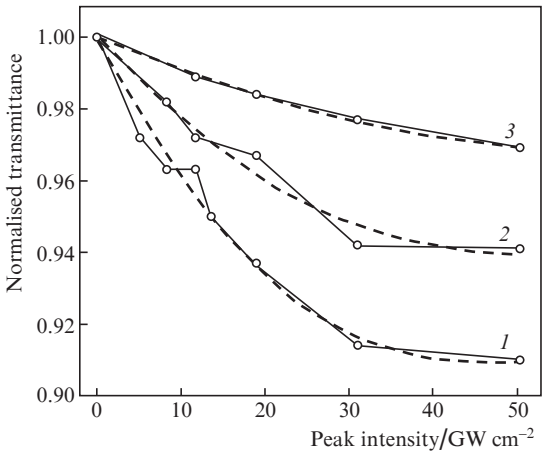

Figure 5. Experimental dependences of the normalised transmittance on the peak intensity of incident radiation for perovskites films (*1*) $MA_{0.15}FA_{0.75}Cs_{0.1}PbI_3$ (L = 45 nm), (*2*) $MAPbI_3$ + 1% PVC (L = 65 nm), and (*3*) $CsPbI_2Br$ (L = 120 nm); circles are experimental data, and dashed lines are the best approximations obtained using expression (9).

The TPA coefficients found in this study correspond (in order of magnitude) to the coefficients measured in [7, 14–17]. However, the saturation intensities are significantly different. It follows from Table 1 that, under nanosecond excitation conditions, the nonlinear absorption is saturated at intensities $I_s = 0.6–1$ GW cm^{-2} for $MAPbI_3$, whereas in the case of femtosecond excitation saturation occurs at $I_s = 48 \pm 4$ GW cm^{-2} for $MA_{0.15}FA_{0.75}Cs_{0.1}PbI_3$ and 55 ± 8 GW cm^{-2} for $MAPbI_3$ + 1% PVC. Since the optical saturation is determined mainly by the energy flux (specifically, the product $I_s\tau_0$), the saturation intensity should be higher for shorter pulses. This suggestion is confirmed by expression (6). According to it, for films of the same composition with identical TPA cross sections, a decrease in the pulse duration from 1 ns to 400 fs should lead to an increase in the saturation intensity by a factor of 50; this is in agreement with the data of Table 1 for $MAPbI_3$ films ($I_s = 0.6–1$ GW cm^{-2} for τ_0 = 1 ns and $I_s = 55 \pm 8$ GW cm^{-2} for τ_0 = 400 fs).

An inverse dependence of the nonlinear absorption coefficient on the film thickness is observed for perovskite films of the same type. For example, in the films of organometallic perovskites with the ternary cation $(MA_{0.15}FA_{0.75}Cs_{0.1})^+$, the coefficient β_0 changed from 38 to 928 cm GW^{-1} with a change in the film thickness from 350 to 45 nm. In the films of inorganic perovskite $CsPbI_2Br$ the coefficient β_0 changed from 6 to 50 cm GW^{-1} with a change in the film thickness from 300 to 120 nm. A similar dependence of the nonlinear absorption coefficient on the film thickness was observed in [14], where the TPA coefficient changed from 4.73 to 10.94 cm GW^{-1} with a change in the film thickness from 195.4 to 104.6 nm for $CsPbBr_3$, as well as in [15, 16], where a change in the TPA coefficient from 1100 to 9000 cm GW^{-1} with a change in the film thickness from 250 to 90 nm was found for $MAPbI_3$. One of possible factors determining this dependence is the more planar distribution of crystallites in the thinnest films in comparison with the more stochastic distribution in the thickest films. The probe polarisation vector lies in the substrate plane and, therefore, in the crystallite-distribution plane in the thinnest films, due to which the two-photon transition probability increases.

As follows from the data of Table 1, in the case of perovskite films with thicknesses ranging from 45 to 120 nm, the coefficient β_0 for the samples with a mixed cation (524 ± 48 cm GW^{-1} for $MAPbI_3$ + 1% PVC and 928 ± 52 cm GW^{-1} for $MA_{0.15}FA_{0.75}Cs_{0.1}PbI_3$) greatly exceeds that for the film of inorganic perovskite $CsPbBr_3$: 50 cm GW^{-1}. The same regularity is observed for thick perovskite films. In particular, for the (300–350)-nm films, the coefficient β_0 is higher for the perovskite with a mixed cation ($MA_{0.15}FA_{0.75}Cs_{0.1}PbI_{2.85}Br_{0.15}$) and lower for the inorganic perovskite $CsPbBr_3$: 38 ± 1.7 and 6 ± 2.0 cm GW^{-1}, respectively.

We could not find out experimentally how encapsulation of film samples with a PMMA layer affects their nonlinear properties. We can only state that a perovskite film encapsulated by a PMMA layer has a longer-term stability and is protected better from atmospheric oxygen and humidity; being light-proof, it retains optical properties for few days.

2.3. *Z*-scan measurements at a wavelength of 532 nm

Similar z-scan measurements were performed on the second harmonic (532 nm) with a photon energy E = 2.33 eV, which exceeds the perovskite band gap (E_g = 1.49–1.79 eV). The second-harmonic pulse duration was 300 fs, and the pulse energy was 150 nJ at a pulse repetition rate of 10 kHz. The

Table 1. Parameters of nonlinear optical absorption of perovskite films under pulsed excitation at a wavelength of 1064 nm.

Samole	β_0/cm GW^{-1}	I_s/GW cm^{-2}	τ_0/fs	L/nm	References
$MA_{0.15}FA_{0.75}Cs_{0.1}PbI_3$	928 ± 52	48 ± 4	400	45	this study
$MA_{0.15}FA_{0.75}Cs_{0.1}PbI_{2.85}Br_{0.15}$	38 ± 1.7	>80	400	340–350	this study
$MAPbI_3$ + 1% PVC	524 ± 48	55 ± 8	400	65	this study
$CsPbI_2Br$	50 ± 2.0	>80	400	120	this study
$CsPbI_2Br$	6 ± 2.0	–	400	300	this study
$MAPbI_3$	7000–9000	0.6–1	10^6	90	[15]
$MAPbI_3$	1100–1500	0.6–1	10^6	250	[16]

samples under study became bleached during *z*-scanning with an increase in intensity in the beam waist region. The bleaching signal was not reproduced and increased with each next sample passage through the waist region. Figure 6 shows experimental *z*-scan signals from the $MA_{0.15}FA_{0.75}Cs_{0.1}PbI_3$ film sample, recorded after different numbers of passages through the waist region. It can be seen that the transmittance increases after each sample passage through the waist region, a fact suggesting that irreversible photochemical changes occur in the sample in the illumination zone. To confirm the photochemical degradation of a perovskite film exposed to intense light at a wavelength of 532 nm, we investigated the bleaching kinetics for a film sample located in the waist region. Figure 7 shows the experimental kinetics of the increase in intensity on the detecting photodiode in dependence of the exposure time.

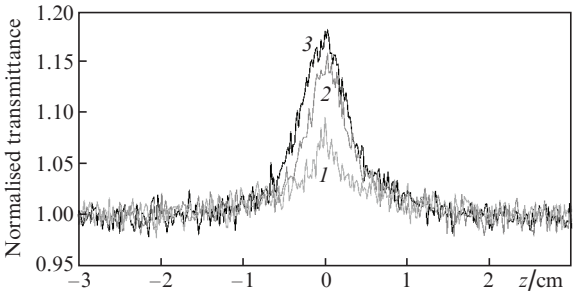

Figure 6. Normalised transmittance for the $MA_{0.15}FA_{0.75}Cs_{0.1}PbI_3$ film ($L = 45$ nm) at a probe wavelength of 532 nm and pulse energy of 130 nJ for different numbers of sample passages through the beam waist region: (*1*) 1, (*2*) 4, and (*3*) 10.

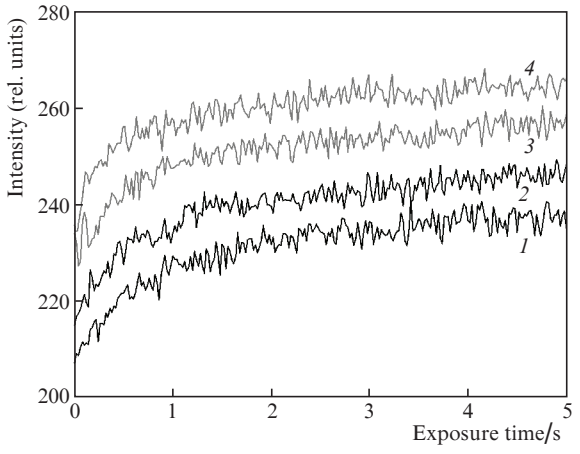

Figure 7. Photodegradation kinetics for perovskite films (*1*) $MA_{0.15}FA\,Cs_{0.1}PbI_3$, (*2*) $MAPbI_3$ + 1% PVC + PMMA, (*3*) $MAPbI_3$ + 1% PVC, and (*4*) $MA_{0.15}FA_{0.75}Cs_{0.1}PbI_3$ + PMMA, irradiated at a wavelength of 532 nm: dependence of the pulsed radiation intensity transmitted through the film on the exposure time. The average intensity of incident radiation is 53 W cm^{-2}; the peak intensity is 18 GW cm^{-2}.

The sample motion velocity through the waist region in *z*-scan measurements was 0.8 cm s^{-1}. As follows from Fig. 6, the main bleaching signal was recorded for 1 s. It can be seen in Fig. 7 that the sample was bleached to a depth of 7% during the first second, which corresponds exactly to the film normalised transmittance in Fig. 6 after the first passage. The saturation of photodegradation for exposures longer than 1 s (Fig. 7) is also confirmed by further retardation of the signal growth rate at repeated sample passages through the waist region during *z*-scanning (Fig. 6). We can conclude that encapsulation by a PMMA layer does not cause any changes in the photodegradation rate of perovskite films during the first several seconds of exposure. As follows from the bleaching kinetics (Fig. 7), the photodegradation rates of protected and unprotected $MA_{0.15}FA_{0.75}Cs_{0.1}PbI_3$ and $MAPbI_3$ films coincide within the experimental error.

3. Conclusions

Organometallic halide perovskite films irradiated by femtosecond laser pulses at wavelengths of 1064 and 532 nm were studied. The irradiation at a probe wavelength of 1064 nm revealed that the nonlinear absorption coefficient of a film depends on its thickness. Thinner films are characterised by higher nonlinear absorption coefficients. It was shown both theoretically and experimentally that the nonlinear absorption saturation intensity for perovskite films depends on the pump pulse duration and increases with the pump pulse shortening. The experimental values of nonlinear absorption coefficient are larger for the films of organometallic halide perovskites with a mixed cation and smaller for the films of inorganic perovskite $CsPbI_2Br$. It was shown that the signal bleaching for the films irradiated by intense 532-nm light is due to the irreversible photoinduced film degradation. Encapsulation of perovskite films by a PMMA layer does not lead to any changes in their photodegradation rate during the first few seconds of illumination; however, an encapsulated film has a longer-term stability and is better protected from atmospheric oxygen and humidity. In addition, being light-proof, the film retains its optical properties for several days.

Acknowledgements. This work was performed within government research contract No. AAAA-A19-119032690060-9 (L.A.S.).

References

1. Mitzi D.B. *J. Chem. Soc., Dalton Trans*., (1), 1 (2001); https://doi.org/10.1039/B007070J.
2. Weber D. *Z. Naturforsch. B*, **33**, 1443 (1978).
3. Poglitsch A., Weber D. *J. Chem. Phys*., **87**, 6373 (1987).
4. Ferrando A., Martínez-Pastor J.P., Suárez I. *J. Phys. Chem. Lett*., **9**, 5612 (2018).
5. Li P., Chen Y., Yang T., Wang Z., et al. *ACS Appl. Mater. Interfaces*, **9** (14), 12759 (2017).
6. Zhang R., Fan J., Zhang X., Yu H., Zhang H., Mai Y., Xu T., Wang J., Snaith H.J. *ACS Photonics*, **3**, 371 (2016).
7. Saouma F.O., Stoumpos C.C., Wong J., Kanatzidis M.G., Jang J.I. *Nat. Commun*., **8**, 742 (2017).
8. Qi X., Zhang Y., Ou Q., Ha S.T., Qiu C.-W., Zhang H., Cheng Y.-B., Xiong Q., Bao Q. *Small*, **14**, 1800682 (2018).
9. Frolova L.A., Davlethanov A.I., Dremova N.N., Zhidkov I., Akbulatov A.F., Kurmaev E.Z., Aldoshin S.M., Stevenson K.J., Troshin P.A. *J. Phys. Chem. Lett*., **11**, 6772 (2020).
10. Song Z., Wang C., Phillips A.B., Grice C.R., Zhao D., et al. *Sustainable Energy Fuels*, **2**, 2460 (2018).
11. Saliba M., Matsui T., Seo J.Y., Domanski K., et al. *Energy Environ. Sci*., **9**, 1989 (2016).

12. Chen L., Wan L., Li X., Zhang W., Fu S., Wang Y., Li S., Wang H.-Q., Song W., Fang J. *Chem. Mater*., **31**, 9032 (2019).
13. Quilettes D.W., Vorpahl S.M., Stranks S.D., Nagaoka H., Eperon G.E., Ziffer M.E., Snaith H.J., Ginger D.S. *Science*, **348**, 683 (2015).
14. Zhang J., Jiang T., Zheng X., Shen C., Cheng X. *Opt. Lett*., **42**, 3371 (2017).
15. Redondo-Obispo C., Suárez I., Quesada S.J., Ripolles T.S., Martínez-Pastor J.P., et al. *J. Phys. Chem. Lett*., **11**, 2188 (2020).
16. Suarez I., Valles-Pelarda M., Gualdron-Reyes A.F., Mora-Sero I., Ferrando A., Michinel H., Salgueiro J.R., Martínez-Pastor J.P. *APL Mater*., **7**, 041106 (2019).
17. He G.S., Tan L.-S., Zheng Q., Prasad P.N. *Chem. Rev*., **108**, 1245 (2008).